The systematic investigation of energetic-particle-driven geodesic acoustic mode channeling using MEGA code

To cite this article before publication: Hao Wang *et al* 2020 *Nucl. Fusion* in press https://doi.org/10.1088/1741-4326/ab8a04

The systematic investigation of energetic-particle-driven geodesic acoustic mode channeling using MEGA code

Hao WANG (王 灝)[1], Yasushi TODO (藤堂 泰)[1], Masaki OSAKABE (長壁 正樹)[1], Takeshi IDO (井戸 毅)[2], Yasuhiro SUZUKI (鈴木 康浩)[1]

[1]National Institute for Fusion Science, National Institutes of Natural Sciences, Toki, Japan

[2]Research Institute for Applied Mechanics, Kyushu University, Kasuga, Japan

E-mail: wanghao@nifs.ac.jp

November 2019

Abstract. Energetic-particle-driven geodesic acoustic modes (EGAMs) channeling in the Large Helical Device (LHD) plasmas are systematically investigated for the first time using MEGA code. MEGA is a hybrid simulation code for energetic particles interacting with a magnetohydrodynamic (MHD) fluid. In the present work, both the energetic particles and the bulk ions are described kinetically. The EGAM profiles in the three-dimensional form is illustrated. Then, EGAM channeling behaviors are analyzed under different conditions. During the EGAM activities without frequency chirping, EGAM channeling occurs in the linear growth stage but terminates in the decay stage after the saturation. During the EGAM activities with frequency chirping, EGAM channeling occurs continuously. Also, low-frequency EGAM makes the energy transfer efficiency (E_{ion}/E_{EP}) higher, and this is confirmed by changing the energetic particle pressure, energetic particle beam velocity, and energetic particle pitch angle. Moreover, higher bulk ion temperature makes the energy transfer efficiency higher. In addition, under a certain condition, the energy transfer efficiency in the deuterium plasma is lower than that in the hydrogen plasma.

1. Introduction

Geodesic acoustic mode (GAM) is an oscillatory zonal flow coupled with density and pressure perturbations in toroidal plasmas[1–6]. In the past years, energetic-particle-driven GAM (EGAM) has been observed in JET, DIII-D, Large Helical Device (LHD), HL-2A, ASDEX-Upgrade, and TCV[7–14]. Many papers have been devoted to various aspects of EGAMs. For example, the basic properties including dispersion relations and resonant conditions[15–33], the continuum damping effect and Landau damping effect[16, 34–37], the different frequency branches[15, 16, 38–41], and the subcritical EGAM instabilities[42–44] were studied. In the DIII-D experiment, the neutron

emission drops during the EGAM activities suggest energetic ion losses[9]. Also, in the LHD experiment, anomalous bulk ion heating during the EGAM activity suggests the existence of EGAM channeling[45]. In addition, EGAMs interact with turbulence and thus affect the plasma transport and confinement[46, 47]. Thus, the understanding of the EGAMs is important for magnetic confinement fusion, because the energetic particles need to be well confined and the bulk plasma heating efficiency should be enhanced.

The EGAM channeling phenomenon has excited the interest of many researchers because of the direct significance for plasma heating. The energy channel of GAM was discussed within the framework of quasilinear theory, and the possibility of the GAM channeling was proved for the first time in Ref.[48]. Then the energy transfer between particles and mode were simulated with a flat equilibrium profile for the first time[49]. In LHD, after observing the EGAM channeling for the first time[45], another investigation was made to find the relation between EGAM channeling and the shear of safety factor[50]. Also, various simulations are devoted to the EGAM channeling phenomena. The mechanism of EGAM channeling based on a realistic LHD configuration was clarified for the first time using MEGA code[51], and the energy transfer during EGAM activities in ASDEX-Upgrade is analyzed using ORB5 and GENE codes[52, 53]. However, at present, the systematic investigation of EGAM energy channel has not been carefully conducted, and thus, it is difficult for experimentalists to reproduce the EGAM channeling in various devices. In LHD, the EGAM phenomena were observed only under the low density conditions but not under the normal density or high density conditions. The present paper is devoted to the systematic investigation of the EGAM channeling under different conditions, and is organized as follows. In section 2, the simulation model and conditions are described. In section 3, the EGAM profile in three-dimensional form is shown, and the bulk ion heating efficiency during EGAM activities under different cases are compared. In section 4, the main conclusions are summarized.

2. Simulation model and parameters

A hybrid simulation code MEGA[54–59] for energetic particles interacting with a magnetohydrodynamic (MHD) fluid is used for the simulations of EGAMs. The hybrid model is widely used in the fusion community[60]. There are two versions of MEGA. In the conventional version, only the energetic particles are described by the kinetic equations, while in the extended version both the energetic particles and the thermal ions are described kinetically. The simulation of the EGAM channeling is conducted with the extended version, and the simulation model in the present work is the same as Ref. [57] and Ref. [51]. This kinetic description of bulk ions is very important for EGAM channeling simulation, because the Landau damping process is a kind of wave-particle interaction process, and this process can be well simulated by the kinetic thermal ions model. The following equations in the extended model[51] are different from those in

the conventional model:

$$\rho\frac{\partial}{\partial t}\mathbf{u_{E\perp}} = -(\mathbf{M}\cdot\nabla)\mathbf{u_{E\perp}} - \nabla p_e + (\mathbf{j} - \frac{Z_i e}{m_i}\rho_i\mathbf{v_{pi}} - \frac{Z_h e}{m_h}\rho_h\mathbf{v_{ph}})\times\mathbf{B}, \quad (1)$$

$$\mathbf{E} = -\mathbf{u_{E\perp}}\times\mathbf{B} + \frac{\nabla_\parallel p_e}{(-e)n_e} + \eta(\mathbf{j}-\mathbf{j_{eq}}), \quad (2)$$

$$\rho = \rho_i + \rho_h, \quad (3)$$

$$\mathbf{M} = \rho\mathbf{u_{E\perp}} + (\rho_i v_{i\parallel} + \rho_h v_{h\parallel})\mathbf{b} + \rho_i\mathbf{v_{pi}} + \rho_h\mathbf{v_{ph}}, \quad (4)$$

$$\rho_i\mathbf{v_{pi}} = \frac{m_i}{Z_i e}(-\frac{\nabla p_{i\perp}\times\mathbf{B}}{B^2} + (p_{i\parallel}-p_{i\perp})\frac{\nabla\times\mathbf{b}}{B}), \quad (5)$$

$$\rho_h\mathbf{v_{ph}} = \frac{m_h}{Z_h e}(-\frac{\nabla p_{h\perp}\times\mathbf{B}}{B^2} + (p_{h\parallel}-p_{h\perp})\frac{\nabla\times\mathbf{b}}{B}). \quad (6)$$

The subscript h denotes the hot particles. In the present work, hot particles represent energetic particles. We avoid using subscript EP to keep consistent with previous literature. The subscript i denotes the bulk ions. The subscript eq denotes equilibrium state. Equation (1) is momentum equation, and Eq.(2) is Ohm's law. The particle-in-cell (PIC) method is applied for ρ_i, ρ_h, $\rho_i v_{i\parallel}$, $\rho_h v_{h\parallel}$, $p_{i\parallel}$, $p_{i\perp}$, $p_{h\parallel}$, and $p_{h\perp}$. The collisions are not modeled in the PIC scheme of the present simulation, thus the bulk ions do not absorb energy from energetic particles via collision processes. This is reasonable because the beam velocity is higher than critical velocity, and then, the collisions between energetic particles and bulk ions are negligible[61]. A similar model can also be found in Ref. [19].

A realistic 3-dimensional equilibrium generated by HINT code is used for the simulation[62]. This equilibrium data is the same as that in Ref. [51], based on the LHD shot #109031 at time $t = 4.94$ s. At this moment, the EGAM activity is very strong[45], thus it is appropriate for reproducing the EGAM phenomenon. The following four parameters for the EGAM simulation are based on an LHD experiment[45]: 1) The plasma major radius $R_0 = 3.75$ m. 2) The magnetic field strength on the magnetic axis $B_0 = 1.5$ T. 3) The electron density in plasma center $n_e = 0.072\times10^{19}$ m^{-3}, and density profile is the same as the experiment. And finally, 4) The safety factor $q = 2.82$ on the magnetic axis, and $q = 0.83$ on the plasma edge. Hydrogen plasma is assumed, that is the same as the experiment. But in order to investigate the isotope effects, deuterium plasma is also considered in a case. Also, to make the parameter scan, the parameter of the injected neutral beam energy E_{NBI} is not always the same as the realistic value 170keV. In addition, a Gaussian-type pitch angle distribution function

$$f(\Lambda) = \exp[-\frac{(\Lambda-\Lambda_{peak})^2}{\Delta\Lambda^2}] \quad (7)$$

is assumed for the energetic particles, where $\Lambda = \mu B_0/E$ is the pitch angle variable, μ is the magnetic moment, E is the particle energy, Λ_{peak} represents the pitch angle for the distribution peak, and $\Delta\Lambda$ is a parameter to control the distribution width. Similar

to E_{NBI}, Λ_{peak} is not always the realistic value 0.1. A slowing-down energetic particle distribution function and a Maxwellian bulk ion distribution are assumed in the paper.

The number of computational particles is 8 million for both energetic particles and bulk ions, but in some cases, a larger number of particles, 67 million, is also used to decrease the noise. Cylindrical coordinates (R, ϕ, z) are employed. For LHD equilibrium, there are ten pitches in the toroidal direction (ϕ direction). Since the toroidal mode number of the GAM is $n = 0$, for simplicity, only one pitch from $\phi = 0$ to $\phi = 0.2\pi$ is used for the present simulation, while the other nine pitches from $\phi = 0.2\pi$ to $\phi = 2\pi$ are obtained by periodic extension. This simplification is valid as shown in Ref. [44, 51], and the simplification saves a considerable amount of computational resources and time. The numbers of grid points of this pitch in the (R, ϕ, z) directions are (128, 64, 128), respectively.

3. Simulation results

3.1. Mode profiles in three-dimensional form

The simulated mode profile of pressure perturbation δP is shown in Fig. 1. In the top part of the figure, the plasma shape in LHD is shown, and the four slices represent the poloidal cross sections at different ϕ positions. In the bottom part of the figure, the poloidal cross section at four different times or four different phases are shown in the map views. From left to right, the first map view cross section represents δP at the initial phase or phase equals to 0, and the perturbation is almost zero. The second map view cross section represents δP at phase equals to $\pi/2$, and the perturbation is very strong. The green color represents the positive δP, while the red color represents the negative δP. The third map view cross section represents δP at phase equals to π. The perturbation is almost zero, and this cross section and the first cross section are in anti-phase. The last map view cross section (inside the rectangle with black boundary) represents δP at phase equals to $3\pi/2$, and the perturbation is very strong. This cross section and the second cross section are in anti-phase. The two rectangles with black boundary represent original size and enlarged size, respectively.

This mode peaks in the core region, very close to the plasma center. The mode width is very large, and that means the simulated mode is a global mode. It is very clear that the poloidal mode number is $m = 1$. The mode profile properties are consistent with the nature of GAM and EGAM[1, 2, 15, 22].

3.2. EGAM channeling with and without frequency chirping

EGAM channeling with and without frequency chirping performs differently, as shown in Fig. 2. Fig. 2(a) and (b) show the case with energetic particle pressure $\beta_{EP} = 0.08\%$. Fig. 2(a) shows the energy evolution of energetic particles and bulk ions. Fig. 2(b) shows the evolution of amplitude (solid line) and frequency (line with points). The simulation time is only 0.25 ms, thus the width of time window is not sufficient to show

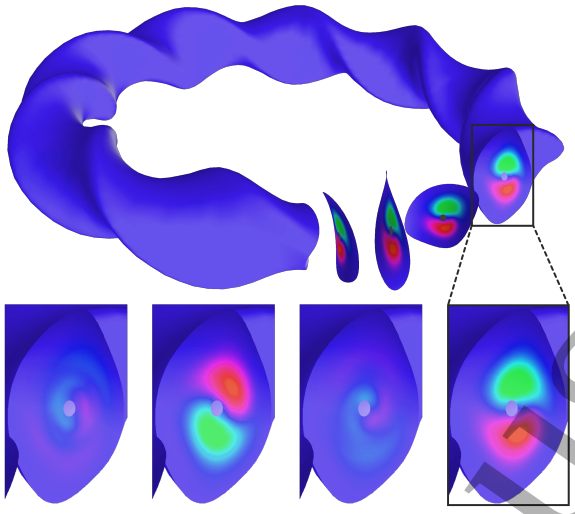

Figure 1. The simulated mode profile of pressure perturbation in three-dimensional form.

the evolution of frequency spectrum with good frequency resolution. Instead of the fast Fourier transform (FFT), the mode frequency is simply evaluated by $f = 1/T$, where T is period and calculated by the time interval between the points of $v_\theta = 0$, that means, the cross points of the solid line (v_θ) and $v_\theta = 0$ straight line. The frequency is approximately constant at 40 kHz. The plotted frequency is in the range between 36 kHz and 44 kHz. The disturbance of frequency is caused by strong wave-particle interactions. In the case without frequency chirping, the energy channel is established in linear growth phase and saturated phase, but after the saturation, the mode starts to decay at 0.14 ms and the energy channel is closed. In decay phase, the energetic particles hardly lose energy, and the bulk ions do not absorb energy.

Figure 2(c) and (d) show the case with $\beta_{EP} = 0.04\%$. It is the same case as Fig. 4 of Ref. [51], but plotted in different forms. Fig. 2(c) shows the energy evolution of energetic particles and bulk ions. Fig. 2(d) shows the evolution of amplitude (solid line) and frequency (line with points). In order to maintain the consistency with Fig. 2(b), the frequency of Fig. 2(d) is evaluated by $f = 1/T$, not by FFT as shown in Fig. 4 of Ref. [51]. The mode frequency is kept constant in the linear growth phase. Then, in nonlinear saturated phase, the frequency changes between 50 kHz and 64 kHz, but the frequency tendency is chirping up. This result is the same as Fig. 4 of Ref. [51]. In the frequency chirping phase, energetic particles lose energy continuously, and the bulk ions absorb energy continuously. This suggests that the energy channel is always maintained by EGAM.

The above difference can be interpreted by Ref. [51]. In Ref. [51], the clump of bulk ions are created, and the particles in the clump keep resonant with the mode during the frequency chirping. Thus, the bulk ions can absorb energy continuously via resonance. But for the mode without frequency chirping, the resonance can not be maintained in the nonlinear phase. Thus, when the decay of the mode starts, the energy channel closes

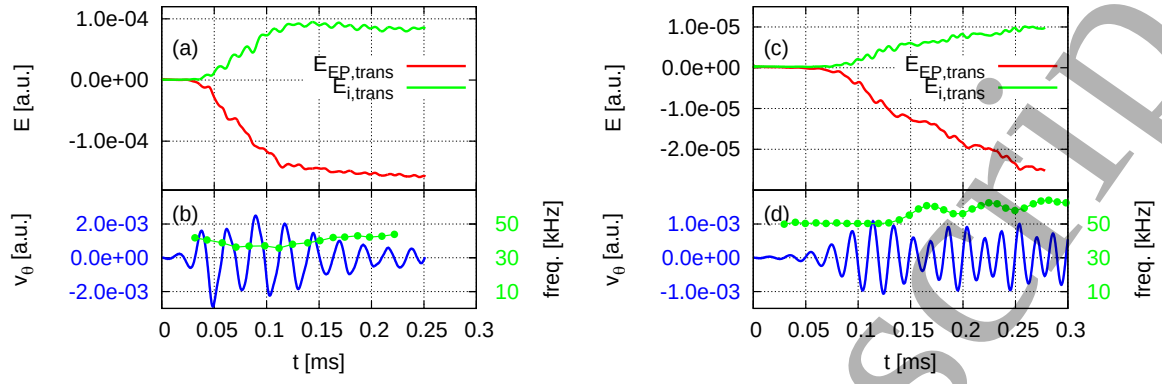

Figure 2. The energy evolution of energetic particles and bulk ions with (a) $\beta_{EP} = 0.08\%$ and (c) $\beta_{EP} = 0.04\%$. The poloidal velocity v_θ time evolution (solid lines) and frequency (lines with points) are also shown with (b) $\beta_{EP} = 0.08\%$ and (d) $\beta_{EP} = 0.04\%$.

at once, and then, the bulk ions can not absorb any energy.

3.3. Time evolution of energy transfer efficiency

Both the energy absorbed by bulk ions E_{ion} and the energy lost from energetic particles E_{EP} changes together. Then, a question may arise regarding how the energy transfer efficiency E_{ion}/E_{EP} changes with time. In order to illustrate the time evolution of energy transfer efficiency, Fig. 3 is plotted. In Fig. 3(a), the energy transfer of bulk ions and energetic particles are plotted with solid curves. They change from almost 0 to 1.3×10^{-5} and -3.0×10^{-5}, respectively. The energy evolution perturbs because of the wave-particle interactions. The dashed curve represents a coefficient k multiplied by the energy transfer of energetic particles, where $k = -0.47$. It is very clear that in Fig. 3 the energy transfer efficiency $E_{ion}/E_{EP} = 0.47$ and this value does not change with time because 1) the dashed curve and the solid curve coincide from the beginning to the end, and 2) the coefficient k is a constant which does not change with time. Similar conclusions can also be made from Fig. 2, although the dashed curves are not plotted to keep the figure clean. In Fig. 2(a), from $t = 0$ to $t = 0.14$ ms, the energy transfer efficiency is always 0.61. After $t = 0.14$ ms, the energy channel is closed and thus the bulk ions do not absorb energy. In Fig. 2(c), from beginning to the end, the energy transfer efficiency is always 0.42.

3.4. Energy transfer efficiency and mode frequency

It is claimed that the EGAM channeling is caused by sideband resonance[51], then, energy transfer efficiency should increase with the decrease of mode frequency. In order to confirm that, three figures are plotted for demonstration. Fig. 4 shows the energy transfer efficiency and mode frequency versus energetic particle pressure. The energy transfer efficiency increases with the energetic particle pressure, while the mode

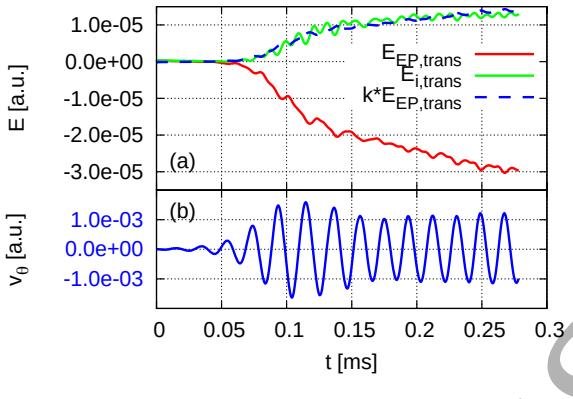

Figure 3. (a) The time evolution of energy transfer of bulk ions and energetic particles (solid curves). The dashed curve represent a constant k multiplied by the energy transfer of energetic particles where $k = -0.47$. (b) The poloidal velocity v_θ time evolution.

frequency decreases with the increase of the energetic particle pressure. In other words, the energy transfer efficiency increases with the decrease of mode frequency. Fig. 5 shows the energy transfer efficiency and mode frequency versus energetic particle beam energy or beam velocity. The energy transfer efficiency decreases with the increase of energetic particle beam energy, while the mode frequency increases with beam energy. In other words, again, the energy transfer efficiency increases with the decrease of mode frequency. Fig. 6 shows the energy transfer efficiency and mode frequency versus energetic particle pitch angle Λ_{peak}. The energy transfer efficiency increases with Λ_{peak}, while the mode frequency decreases with the increase of Λ_{peak}. Again, the energy transfer efficiency increases with the decrease of mode frequency. This figure suggests that the EGAM is a kind of energetic-particle-driven mode (EPM) whose frequency is determined by energetic particles. The result is similar to Fig. 10 of Ref. [39], but in the present work, the mode frequency changes only approximately 10% by changing Λ_{peak}, while in Fig. 10 of Ref. [39], the frequency changes approximately 40%. In the present work, the simulated EGAM is the low-frequency branch, while the mode in Ref. [39] is the high-frequency branch. The high-frequency branch is a kind of beam branch[16], it is weakly coupled to the GAM continuum and more easily to be affected by energetic particles.

The lower frequency EGAMs make energy transfer efficiency higher because the interactions between lower frequency mode and bulk ions are stronger. In experiment, the higher energetic particle pressure (or higher NBI power), the lower NBI velocity, and the higher number of perpendicular injected particles may be helpful for better observation of EGAM channeling. But the energetic particle pressure should not be too high, otherwise, the EGAM may be excited rapidly without frequency chirping, and then the EGAM energy channel may close in a very short time.

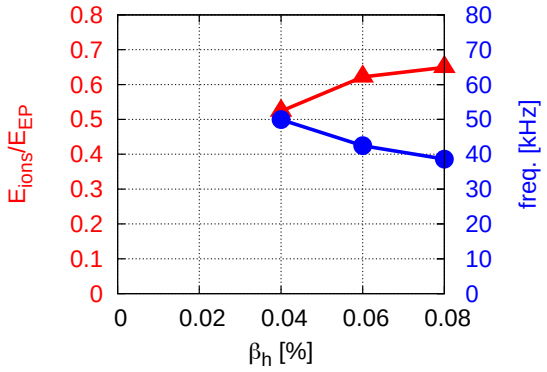

Figure 4. The energy transfer efficiency (line with triangle) and EGAM frequency (line with circle) versus energetic particle pressure. The subscript "h" represents hot particles (equivalent to energetic particles).

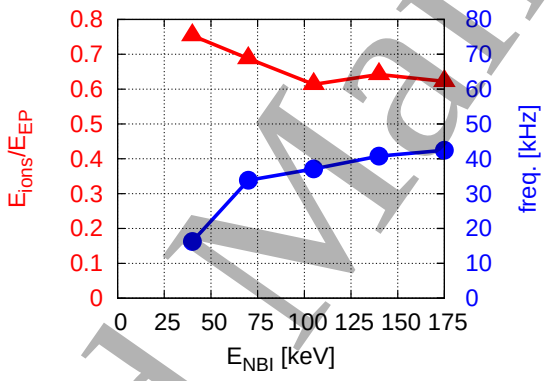

Figure 5. The energy transfer efficiency (line with triangle) and EGAM frequency (line with circle) versus energetic particle beam energy or beam velocity. The subscript "NBI" represents neutral beam injection.

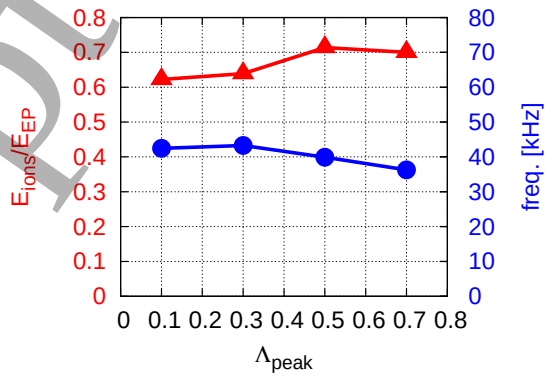

Figure 6. The energy transfer efficiency (line with triangle) and EGAM frequency (line with circle) versus energetic particle pitch angle Λ_{peak}.

3.5. Energy transfer efficiency and plasma temperature

In addition to decreasing EGAM frequency, another possible way to increase energy transfer efficiency is increasing transit frequency of bulk ions, or, increasing bulk plasma temperature. Fig. 7 shows the energy transfer efficiency and mode frequency versus square root of bulk ion temperature T_i. The open triangle and circles represent the cases with central peaked ion temperature profile, but this profile induces some numerical instabilities for very low ion temperature cases. Thus, some other cases with uniform ion temperature profiles are used to demonstrate the dependence of T_i as shown by closed triangles and circles. The energy transfer efficiency increases with T_i. Also, the mode frequency linearly increases with $\sqrt{T_i}$. The increase of $\sqrt{T_i}$ (or bulk ion transit frequency $f_{tr,ion}$) is faster than the increase of mode frequency f_{EGAM}, and thus, the ratio of $f_{tr,ion}/f_{EGAM}$ increases and the energy transfer efficiency increases. The frequencies of open circles and closed circles are very close to each other, because the EGAM frequency is mainly determined by energetic particles, not by plasma profiles. The closed triangles are higher than the open triangles, because for the closed triangles, the bulk ions near the edge region can also absorb energy, and then, the energy transfer efficiencies increase.

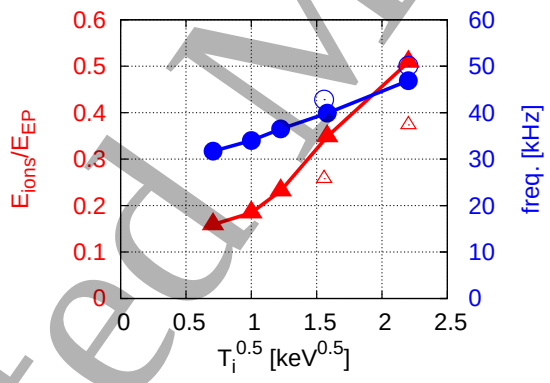

Figure 7. The energy transfer efficiency (line with closed triangle) and EGAM frequency (line with closed circle) versus square root of bulk ion temperature $\sqrt{T_i}$ with uniform ion temperature profile. The open triangles and circles represent the cases with central peaked ion temperature profile.

In experiment, the higher bulk ion temperature or the wider bulk ion temperature profile may be helpful for better observation of EGAM channeling.

3.6. Energy transfer efficiency and dissipation coefficients

The dissipation coefficients includes viscosity ν, diffusivity ν_n, and resistivity η. They appear in MHD equations of MEGA code[22, 54–56, 58]. In the present work, the dissipation coefficients ν, ν_n, and η/μ_0 are assumed to be equal to each other, where μ_0 is the vacuum magnetic permeability. The dissipation coefficients are useful to maintain numerical stability, and the dissipation terms play a physical role in enhancing the

damping of EGAMs. These coefficients affect both the mode amplitude and the energy transfer efficiency, as shown in Fig. 8. Both the energy transfer efficiency and the mode amplitude decrease with the dissipation coefficients. More energy dissipates by increasing the dissipation coefficients, and thus, less energy can be transferred to the bulk ions. In the experiment, the value of resistivity η is approximately $10^{-9}\ \Omega\cdot$m or $10^{-8}\ \Omega\cdot$m, but in Fig. 8, the range of η is from $1.8\times10^{-5}\ \Omega\cdot$m to $1.6\times10^{-4}\ \Omega\cdot$m. In the present simulation, the numerical stability can not be maintained if lower values of η are applied. Then, it becomes impossible to quantitatively compare the simulated energy transfer efficiency with the experiment.

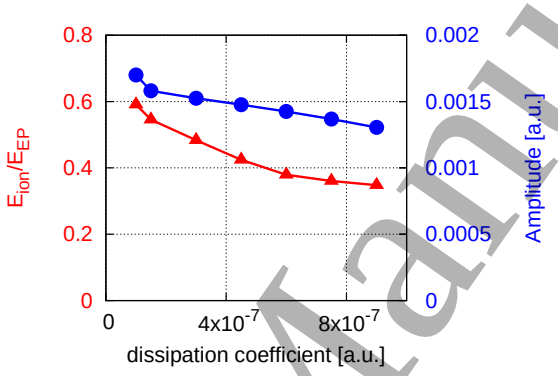

Figure 8. The energy transfer efficiency (line with triangle) and EGAM amplitude (line with circle) versus dissipation coefficients.

3.7. Isotope effect

Isotope effect is important for burning plasma. Then, Fig. 9(a) shows the energy transfer efficiency and mode frequency versus plasma mass number. The EGAM frequency in deuterium plasma is lower than that in hydrogen plasma because the acoustic wave speed varies inversely with the square root of ion mass. The energy transfer efficiency in deuterium plasma is also lower than that in hydrogen plasma, which is difficult to explain. In the simulation of deuterium plasma, the mass number changed by the factor of 2, and the beam energy E_{NBI} remains 170 keV. Thus, the orbit width is changed by the factor of $\sqrt{2}$, and accordingly, many basic properties are changed. Then, it is not appropriate to directly compare the energy transfer efficiency. Also, the three-dimensional configuration and the profiles of density and temperature are based on a realistic low density hydrogen plasma discharge, but in the deuterium plasma discharge, the configuration and the profiles are different. Then, again, it is not appropriate to directly compare the energy transfer efficiency. Fig. 9(b) shows the mode profiles of $m/n = 0/0$ component in hydrogen plasma and deuterium plasma. The other components are negligible, as shown in Fig. 1 of Ref. [51]. In the deuterium plasma, the mode width becomes larger, and thus, the energetic particle redistribution and loss become easier. The EGAM may be worse in deuterium plasma for more particle loss and less energy transfer in the present case.

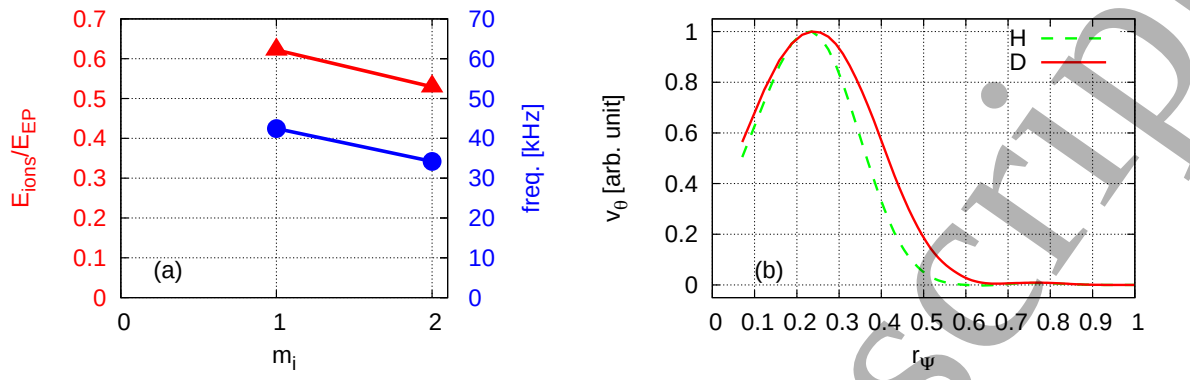

Figure 9. (a) The energy transfer efficiency (line with triangle) and EGAM amplitude (line with circle) versus dissipation coefficients. (b) The mode profiles of $m/n = 0/0$ component in hydrogen plasma and deuterium plasma.

4. Summary

The properties of EGAM channeling are systematically investigated for the first time, and mode profiles in three-dimensional form are presented. Six conclusions are found as follows. First, during the EGAM activities without frequency chirping, EGAM channeling occurs in the linear growth stage but terminates in the decay stage after saturation. During the EGAM activities with frequency chirping, EGAM channeling occurs continuously in both linear growth stage and nonlinear saturated stage. Second, during the existence of the EGAM energy channel, the bulk ion heating power increases with time, but the energy transfer efficiency (E_{ion}/E_{EP}) does not change because both the energy absorption of bulk ions and the energy loss of energetic particles change together. Third, lower frequency EGAMs make energy transfer efficiency higher because the interactions between lower frequency mode and bulk ions are stronger. This is confirmed by changing the parameters of energetic particle pressure, energetic particle beam energy, and energetic particle pitch angle. Fourth, higher bulk ion temperature makes energy transfer efficiency higher because the transit frequency of bulk ions $f_{tr,ion}$ is higher, and thus, more bulk ions are resonant with mode and absorb energy. Fifth, the energy transfer efficiency increases with the decrease of dissipation coefficients. Less energy dissipates by decreasing the dissipation coefficients, and thus, more energy can be transferred to the bulk ions. Last, the isotope effect is analyzed with a hydrogen plasma configuration and with the hydrogen plasma density and temperature profiles. Under these conditions, the energy transfer efficiency in the deuterium plasma is lower than in the hydrogen plasma.

In experiment, the higher NBI power, the lower NBI velocity, the higher number of perpendicular injected particles, the higher bulk ion temperature, and the wider bulk ion temperature profile are probably applicable strategies for improving observation of EGAM channeling. Also, it is possible that EGAM channeling can be more easily observed in hydrogen plasma than that in deuterium plasma.

Acknowledgments

Numerical computations were performed on the "Plasma Simulator" (FUJITSU FX100) of National Institute for Fusion Science (NIFS) with the support and under the auspices of the NIFS Collaboration Research program (NIFS18KNST136, NIFS18KNXN365, and NIFS19KNXN397), and the "K Computer" of the RIKEN Advanced Institute for Computational Science (Project ID: hp180200). This work was partly supported by MEXT as "Priority Issue on Post-K Computer" (Accelerated Development of Innovative Clean Energy Systems), JSPS KAKENHI Grant No. JP15K06652, No. JP18K13529, No. JP18H01202, and "PLADyS", JSPS Core-to-Core Program, A. Advanced Research Networks. The authors thank Prof. H. Sugama, Prof. K. Toi, Dr. K. Shinohara, Dr. Ph. Lauber, Prof. Z. Qiu, and Prof. D. Zarzoso for fruitful discussions.

References

[1] Winsor N, Johnson J and Dawson J 1968 *Physics of Fluids* **11** 2448 ISSN 0031-9171 URL http://dx.doi.org/10.1063/1.1691835

[2] Diamond P H, Itoh S I, Itoh K and Hahm T S 2005 *Plasma Physics and Controlled Fusion* **47** R35–R161 ISSN 1361-6587 URL http://dx.doi.org/10.1088/0741-3335/47/5/R01

[3] Watari T, Hamada Y, Notake T, Takeuchi N and Itoh K 2006 *Physics of Plasmas* **13** 062504 (*Preprint* https://doi.org/10.1063/1.2206170) URL https://doi.org/10.1063/1.2206170

[4] Sugama H and Watanabe T H 2006 *Physics of Plasmas* **13** 012501 ISSN 1089-7674 URL http://dx.doi.org/10.1063/1.2149311

[5] Zonca F and Chen L 2008 *EPL (Europhysics Letters)* **83** 35001 URL https://doi.org/10.1209%2F0295-5075%2F83%2F35001

[6] Chen L, Qiu Z and ZoncaF 2014 *Europhysics Letters* **107** 15003 (*Preprint* https://doi.org/10.1209/0295-5075/107/15003) URL https://doi.org/10.1209/0295-5075/107/15003

[7] Berk H, Boswell C, Borba D, Figueiredo A, Johnson T, Nave M, Pinches S, Sharapov S and contributors J E 2006 *Nuclear Fusion* **46** S888–S897 URL https://doi.org/10.1088%2F0029-5515%2F46%2F10%2Fs04

[8] Boswell C, Berk H, Borba D, Johnson T, Pinches S and Sharapov S 2006 *Physics Letters A* **358** 154 – 158

[9] Nazikian R, Fu G Y, Austin M E, Berk H L, Budny R V, Gorelenkov N N, Heidbrink W W, Holcomb C T, Kramer G J, McKee G R, Makowski M A, Solomon W M, Shafer M, Strait E J and Zeeland M A V 2008 *Phys. Rev. Lett.* **101**(18) 185001 URL https://link.aps.org/doi/10.1103/PhysRevLett.101.185001

[10] Ido T, Shimizu A, Nishiura M, Nakamura S, Kato S, Nakano H, Yoshimura Y, Toi K, Ida K, Yoshinuma M, Satake S, Watanabe F, Morita S, Goto M,

Itoh K, Kubo S, Shimozuma T, Igami H, Takahashi H, Yamada I, Narihara K and the LHD Experiment Group 2011 *Nuclear Fusion* **51** 073046 URL http://stacks.iop.org/0029-5515/51/i=7/a=073046

[11] Chen W, Ding X, Yu L, Ji X, Shi Z, Zhang Y, Zhong W, Yuan G, Dong J, Yang Q, Liu Y, Yan L, Zhou Y, Jiang M, Li W, Song X, Chen S and and X D 2013 *Nuclear Fusion* **53** 113010 URL https://doi.org/10.1088%2F0029-5515%2F53%2F11%2F113010

[12] Horváth L, Papp G, Lauber P, Por G, Gude A, Igochine V, Geiger B, Maraschek M, Guimarais L, Nikolaeva V, Pokol G and the ASDEX Upgrade Team 2016 *Nuclear Fusion* **56** 112003 URL http://stacks.iop.org/0029-5515/56/i=11/a=112003

[13] Lauber P, Geiger B, Papp G, Por G, Pokol G I, Poloskei P Z, Guimarais L, Maraschek M, Igochine V, Hayward-Schneider T, Lu Z, Wang X, Conway G, the ASDEX Upgrade Team and the Eurofusion Enabling Research 'NAT' Team 2018 Strongly non-linear energetic particle dynamics in asdex upgrade scenarios with core impurity accumulation *27th IAEA Fusion Energy Conference Proceedings*

[14] Sharapov S, Garcia-Munoz M, Geiger B and Karpushov A e a 2019 experiments on energetic particle driven instabilities in AUG and TCV plasmas with ECRH and ECCD *16th IAEA Technical Meeting on Energetic Particles in Magnetic Confinement Systems - Theory of Plasma Instabilities*

[15] Fu G Y 2008 *Phys. Rev. Lett.* **101**(18) 185002 URL https://link.aps.org/doi/10.1103/PhysRevLett.101.185002

[16] Qiu Z, Zonca F and Chen L 2010 *Plasma Physics and Controlled Fusion* **52** 095003 URL http://stacks.iop.org/0741-3335/52/i=9/a=095003

[17] Berk H and Zhou T 2010 *Nuclear Fusion* **50** 035007 URL http://stacks.iop.org/0029-5515/50/i=3/a=035007

[18] Qiu Z and Chen L 2011 *Plasma Science and Technology* **13** 257–266 URL https://doi.org/10.1088%2F1009-0630%2F13%2F3%2F01

[19] Zarzoso D, Garbet X, Sarazin Y, Dumont R and Grandgirard V 2012 *Physics of Plasmas* **19** 022102 (*Preprint* https://doi.org/10.1063/1.3680633) URL https://doi.org/10.1063/1.3680633

[20] Fisher R, Pace D, Kramer G, Zeeland M V, Nazikian R, Heidbrink W and García-Muñoz M 2012 *Nuclear Fusion* **52** 123015 URL https://doi.org/10.1088%2F0029-5515%2F52%2F12%2F123015

[21] Kramer G J, Chen L, Fisher R K, Heidbrink W W, Nazikian R, Pace D C and Van Zeeland M A 2012 *Phys. Rev. Lett.* **109**(3) 035003 URL https://link.aps.org/doi/10.1103/PhysRevLett.109.035003

[22] Wang H and Todo Y 2013 *Physics of Plasmas* **20** 012506 ISSN 1089-7674 URL http://dx.doi.org/10.1063/1.4774410

[23] Wang H, Todo Y and Kim C C 2013 *Phys. Rev. Lett.* **110**(15) 155006 URL https://link.aps.org/doi/10.1103/PhysRevLett.110.155006

[24] Ren H and Cao J 2014 *Physics of Plasmas* **21** 122512 (*Preprint* https://doi.org/10.1063/1.4903911) URL https://doi.org/10.1063/1.4903911

[25] Girardo J B, Zarzoso D, Dumont R, Garbet X, Sarazin Y and Sharapov S 2014 *Physics of Plasmas* **21** 092507 (*Preprint* https://doi.org/10.1063/1.4895479) URL https://doi.org/10.1063/1.4895479

[26] Biancalani A, Bottino A, Lauber P and Zarzoso D 2014 *Nuclear Fusion* **54** 104004 URL https://doi.org/10.1088%2F0029-5515%2F54%2F10%2F104004

[27] Ren H 2016 *Nuclear Fusion* **57** 016023 URL https://doi.org/10.1088%2F0029-5515%2F57%2F1%2F016023

[28] Kolesnichenko Y I, Lutsenko V V, Yakovenko Y V, Lepiavko B S, Grierson B, Heidbrink W W and Nazikian R 2016 *Plasma Physics and Controlled Fusion* **58** 045024 URL https://doi.org/10.1088%2F0741-3335%2F58%2F4%2F045024

[29] Qu Z S, Hole M J and Fitzgerald M 2016 *Phys. Rev. Lett.* **116**(9) 095004 URL https://link.aps.org/doi/10.1103/PhysRevLett.116.095004

[30] Sasaki M, Kasuya N, Itoh K, Hallatschek K, Lesur M, Kosuga Y and Itoh S I 2016 *Physics of Plasmas* **23** 102501 (*Preprint* https://doi.org/10.1063/1.4963397) URL https://doi.org/10.1063/1.4963397

[31] Zarzoso D, Migliano P, Grandgirard V, Latu G and Passeron C 2017 *Nuclear Fusion* **57** 072011 URL https://doi.org/10.1088%2F1741-4326%2Faa7351

[32] Biancalani A, Chavdarovski I, Qiu Z, Bottino A, Sarto D D, Ghizzo A, Gurcan O, Morel P and Novikau I 2017 *Journal of Plasma Physics* **83** 725830602

[33] Qu Z S, Hole M J and Fitzgerald M 2017 *Plasma Physics and Controlled Fusion* **59** 055018 URL https://doi.org/10.1088%2F1361-6587%2Faa6636

[34] Qiu Z, Zonca F and Chen L 2012 *Physics of Plasmas* **19** 082507 (*Preprint* https://doi.org/10.1063/1.4745191) URL https://doi.org/10.1063/1.4745191

[35] Palermo F, Biancalani A, Angioni C, Zonca F and Bottino A 2016 *EPL (Europhysics Letters)* **115** 15001 URL https://doi.org/10.1209%2F0295-5075%2F115%2F15001

[36] Biancalani A, Palermo F, Angioni C, Bottino A and Zonca F 2016 *Physics of Plasmas* **23** 112115 (*Preprint* https://doi.org/10.1063/1.4967703) URL https://doi.org/10.1063/1.4967703

[37] Ren H 2017 *Nuclear Fusion* **57** 016023 URL https://iopscience.iop.org/article/10.1088/0029-5515/57/1/016023/meta

[38] Cao J, Qiu Z and Zonca F 2015 *Physics of Plasmas* **22** 124505 (*Preprint* https://doi.org/10.1063/1.4938277) URL https://doi.org/10.1063/1.4938277

[39] Wang H, Todo T, Ido T and Osakabe M 2015 *Physics of Plasmas* **22** 092507 ISSN 1089-7674 URL http://dx.doi.org/10.1063/1.4930130

[40] Ido T, Osakabe M, Shimizu A, Watari T, Nishiura M, Toi K, Ogawa K, Itoh K, Yamada I, Yasuhara R, Yoshimura Y, Kato S and Group T L E 2015 *Nuclear Fusion* **55** 083024 URL http://stacks.iop.org/0029-5515/55/i=8/a=083024

[41] Ren H and Wang H 2018 *Nuclear Fusion* **58** 046005 URL http://stacks.iop.org/0029-5515/58/i=4/a=046005

[42] Ido T, Itoh K, Osakabe M, Lesur M, Shimizu A, Ogawa K, Toi K, Nishiura M, Kato S, Sasaki M, Ida K, Inagaki S and Itoh S I (the LHD Experiment Group) 2016 *Phys. Rev. Lett.* **116**(1) 015002 URL https://link.aps.org/doi/10.1103/PhysRevLett.116.015002

[43] Lesur M, Itoh K, Ido T, Osakabe M, Ogawa K, Shimizu A, Sasaki M, Ida K, Inagaki S, Itoh S I and the LHD Experiment Group 2016 *Phys. Rev. Lett.* **116**(1) 015003 URL https://link.aps.org/doi/10.1103/PhysRevLett.116.015003

[44] Wang H, Todo Y, Ido T and Suzuki Y 2018 *Phys. Rev. Lett.* **120**(17) 175001 URL https://link.aps.org/doi/10.1103/PhysRevLett.120.175001

[45] Osakabe M, Ido T, Ogawa K, Shimizu A, Yokoyama M, Seki R, Suzuki C, Isobe M, Toi K, Spong D A, Nagaoka K, Takeiri Y, Igami H, Seki T, Nagasaki K and the LHD Experiment Group 2014 Indication of bulk-ion heating by energetic particle driven geodesic acoustic modes on LHD *25th IAEA Fusion Energy Conference Proceedings*

[46] Zarzoso D, Sarazin Y, Garbet X, Dumont R, Strugarek A, Abiteboul J, Cartier-Michaud T, Dif-Pradalier G, Ghendrih P, Grandgirard V, Latu G, Passeron C and Thomine O 2013 *Phys. Rev. Lett.* **110**(12) 125002 URL https://link.aps.org/doi/10.1103/PhysRevLett.110.125002

[47] Sasaki M, Itoh K, Hallatschek K, Kasuya N, Lesur M, Kosuga Y and Itoh S I 2017 *Scientific Reports* **7** ISSN 2045-2322 URL http://dx.doi.org/10.1038/s41598-017-17011-y

[48] Sasaki M, Itoh K and Itoh S I 2011 *Plasma Physics and Controlled Fusion* **53** 085017 URL http://stacks.iop.org/0741-3335/53/i=8/a=085017

[49] Zarzoso D, Biancalani A, Bottino A, Lauber P, Poli E, Girardo J B, Garbet X and Dumont R 2014 *Nuclear Fusion* **54** 103006 URL http://stacks.iop.org/0029-5515/54/i=10/a=103006

[50] Toi K, Ogawa K, Ido T, Morita S, Ohdachi S, Pablant N A, Tanaka K, Funaba H, Oishi T, Osakabe M, Shmizu A, Tsuchiya H, Watanabe K Y and LHD Experiment Group 2019 Observation of non-collisional bulk ion heating by energetic ion driven geodesic acoustic modes in LHD *16th IAEA Technical Meeting on Energetic Particles in Magnetic Confinement Systems - Theory of Plasma Instabilities*

[51] Wang H, Todo Y, Oasakabe M, Ido T and Suzuki Y 2019 *Nuclear Fusion* **59** 096041 URL https://doi.org/10.1088%2F1741-4326%2Fab26e5

[52] Novikau I, Biancalani A, Bottino A, Siena A D, Lauber P, Poli E, Lanti E, Villard L, Ohana N and Briguglio S 2019 Implementation of energy transfer technique

in orb5 to study collisionless wave-particle interactions in phase-space (*Preprint* 1903.05024)

[53] Novikau I 2019 Nonlinear dynamics of energetic-particle driven geodesic acoustic modes in ASDEX Upgrade *3rd Asia-Pacific Conference on Plasma Physics*

[54] Todo Y 2006 *Physics of Plasmas* **13** 082503 URL https://aip.scitation.org/doi/citedby/10.1063/1.2234296

[55] Todo Y, Berk H and Breizman B 2010 *Nuclear Fusion* **50** 084016 URL http://stacks.iop.org/0029-5515/50/i=8/a=084016

[56] Todo Y, Seki R, Spong D A, Wang H, Suzuki Y, Yamamoto S, Nakajima N and Osakabe M 2017 *Physics of Plasmas* **24** 081203 ISSN 1089-7674 URL http://dx.doi.org/10.1063/1.4997529

[57] Todo Y 2017 A new magnetohydrodynamic hybrid simulation model with thermal and energetic ions *The 26th International Toki Conference (ITC-26) and The 11th Asia Plasma and Fusion Association Conference(APFA-11)*

[58] Todo Y 2016 *New Journal of Physics* **18** 115005 URL http://stacks.iop.org/1367-2630/18/i=11/a=115005

[59] Sato M and Todo Y 2019 *Nuclear Fusion* **59** 094003 URL https://doi.org/10.1088/1741-4326/ab31f1

[60] Park W, Parker S, Biglari H, Chance M, Chen L, Cheng C Z and Hahm T S 1992 *Physics Fluids B* **4** 2033 URL https://aip.scitation.org/doi/pdf/10.1063/1.860011

[61] Goldston R J and Rutherford P H 1995 *Introduction to plasma physics* (Institute of Physics Publishing) chap 14, pp 229–248

[62] Suzuki Y, Nakajima N, Watanabe K, Nakamura Y and Hayashi T 2006 *Nuclear Fusion* **46** L19 URL http://stacks.iop.org/0029-5515/46/i=11/a=L01